Electronic transport properties in aluminum indium nitride nanorods grown by magnetron sputter epitaxy

Ruei-San Chen, Chih-Che Tang, Ching-Lien Hsiao, Per Olof Holtz and Jens Birch

Original Publication:

Ruei-San Chen, Chih-Che Tang, Ching-Lien Hsiao, Per Olof Holtz and Jens Birch, Electronic transport properties in aluminum indium nitride nanorods grown by magnetron sputter epitaxy, 2013, Applied Surface Science.
http://dx.doi.org/10.1016/j.apsusc.2013.08.102

Electronic Transport Properties in Aluminum Indium Nitride Nanorods Grown by Magnetron Sputter Epitaxy

Ruei-San Chen[1,*], Chih-Che Tang[2], Ching-Lien Hsiao[3], Jens Birch[3]

[1]Graduate Institute of Applied Science and Technology, National Taiwan University of Science and Technology, Taipei 10607, Taiwan

[2]Department of Electronic Engineering, National Taiwan University of Science and Technology, Taipei 10607, Taiwan

[3]Department of Physics, Chemistry, and Biology (IFM), Linköping University, SE-581 83 Linköping, Sweden

*Corresponding author: Prof. Ruei-San Chen

Address: 43, Sec.4, Keelung Rd., Taipei 10607 , Taiwan

TEL: +886-2-2730-3754; Fax: +886-2-2730-3733

E-mail address: rsc@mail.ntust.edu.tw

Abstract

The electronic transport properties of the wide-bandgap aluminum indium nitride (AlInN) nanorods (NRs) with indium composition at ~24% grown by ultrahigh-vacuum magnetron sputter epitaxy (MSE) have been studied. The conductivities of the ternary compound nanostructure locates at the value of 15 $\Omega^{-1}cm^{-1}$, which is respectively one and two orders of magnitude lower than the binary GaN and InN counterparts grown by chemical vapor deposition (CVD). The very shallow donor level/band with the activation energy at 11±2 meV was obtained by the temperature-dependent measurement. In addition, the photoconductivity has also been investigated. The photoconductive (PC) gain of the NRs device can reach near 1000 under a low bias at 0.1 V and the light intensity at 100 Wm^{-2} for ultraviolet response in vacuum. The power-insensitive gain and ambience-dependent photocurrent are also observed, which is attributed to the probable surface-controlled PC mechanism in this ternary nitride nanostructure.

KEYWORDS: aluminum indium nitride, nanorod, photoconductivity, magnetron sputter epitaxy

The Group III-nitride semiconductors, including binary aluminum nitride (AlN), gallium nitride (GaN), and indium nitride (InN), and their ternary compounds have gain substantial attention due to their superior properties for the electronic and optoelectronic device development.[1-3] Among them, the ternary AlInN with the tunable bandgap, which spans near infrared (IR), visible, and deep ultraviolet (UV) ranges, is broader than the other ternary compound such as InGaN and AlGaN. The tunable wide bandgap and lattice constant of AlInN have been utilized for device applications such as light emitting diodes (LEDs),[3] laser diodes (LDs),[4,5] solar-blind photodiodes[6,7], etc. The AlInN has also been used as an excellent barrier layer for optimizing the performance of the high-frequency and high-power high electron mobility transistors (HEMTs).[8-10]

Although the AlInN could offer broad application interest, it is still less studied due to the difficulty in preparing the high-quality crystal ~~with random alloy~~. Recently, growths of the AlInN epitaxial film and especially its quasi one-dimensional (1D) nanostructure have been achieved by the technique of magnetron sputter epitaxy (MSE).[11-13] The achievement has allowed us to investigated the fundamental properties and the potential applications of the novel ternary compound semiconductor. In this letter, we report on the electronic transport properties of the AlInN nanorods (NRs). The dark conductivity and photoconductivity have been investigated by the temperature, power, ambience -dependent measurements. The probable mechanisms for carrier transport in this wide-gap ternary nitride nanostructure are also discussed.

The AlInN NRs were grown on *c*-plane sapphire substrates with and without a vanadium nitride (VN) seed layer at 650 °C and 800 °C , respectively, under 5-mtorr pure nitrogen working pressure by ultrahigh-vacuum magnetron sputter epitaxy. More growth details can be found in our previous publication.[11] The morphology, composition, and

crystallinity of the as-grown AlInN NRs were characterized by the field-emission scanning electron microscopy (FESEM), X-ray diffractometry (XRD), and energy-dispersive X-ray spectroscopy (EDX), respectively. The electrical contact for the AlInN NRs devices which comprise of several or several tens NRs was fabricated by focused-ion beam (FIB) depositions using platinum (Pt) as the contact metal. Electrical measurements were carried out on an ultralow current leakage cryogenic probe station (LakeShore Cryotronics TTP4). A semiconductor characterization system (Keithley 4200-SCS) was utilized to source dc bias and measure current. The He-Cd laser with 325 nm wavelength was used as the UV excitation source for the PC measurements. The incident power of laser was measured by a calibrated power meter (Ophir Nova II) with a silicon photodiode head (Ophir PD300-UV). An UV holographic diffuser was used to broaden laser beam size (~20 mm^2) to minimize the error of the power density calculation.

The typical FESEM image of the MSE-grown high-density AlInN NRs with vertical alignment on the VN(111)/sapphire(001) substrate is shown in Fig. 1(a). The diameter range and the length of the as-grown NRs are 60–120 nm and 3.8 μm, respectively. The crystalline structure and aligned growth can be confirmed by the XRD measurement. Figure 1(b) depicts the XRD pattern with single out-plane orientation of AlInN⟨001⟩, indicating the NR ensembles with hexagonal structure and *c*-axial preferential growth. Upon the position of AlInN(002) diffraction peak ($2\theta = 35.01\pm0.07°$) and the Vegard's law using bulk AlN and InN lattice constants and the deviation parameter,[14] the indium composition (x) of the $Al_{1-x}In_xN$ NRs can be estimated to be 24.2±1.2%. The range of x was further confirmed by the EDX measurement.

The typical dark current versus applied bias (i_d-V) curves measured in the

temperature range of 140–300 K for the AlInN NRs are illustrated in Fig. 2(a). The linear i_d-V behavior shows the stable ohmic contact condition of the NRs device at different temperature. The room temperature conductivity (σ) was estimated at ~15 $\Omega^{-1}cm^{-1}$. While comparing with other III-nitride 1D nanostructures, the value is respectively one and two orders of magnitude lower than the GaN (σ = 150±50 $\Omega^{-1}cm^{-1}$)[15] and InN (σ = 2500 $\Omega^{-1}cm^{-1}$)[16] nanowires (NWs), and is higher than the AlN NWs (σ = 1.6 $\Omega^{-1}cm^{-1}$)[17] grown by the chemical vapor deposition (CVD).

The temperature-dependent σ and its corresponding Arrhenius plot (the inset) are depicted in Fig. 2(b). According to the plot, the σ decreases slightly from 15 to 11 $\Omega^{-1}cm^{-1}$ with the decrease of temperature from 300 to 140 K. The thermal activation energy (E_a) of carrier was calculated by the Arrhenius slope to be ~10 meV. The small E_a is consistent with other three NWs devices with E_a range at 11±2 meV. The AlInN NRs with the small E_a in common indicate the presence of shallow donor levels/bands in this MSE-grown nitride nanostructure.

In addition to dark conductivities, photoconductivities of the AlInN NRs were also characterized. Figure 3(a) depicts the typical photocurrent (i_p) responses to the 325 nm UV illumination under different light intensity (I) in vacuum for the AlInN NRs. The estimated i_p versus I curve is also plotted in Fig. 3(b). Overall, the i_p follows a near linear relationship with the excitation power. To investigate the performance of the NRs photodetector, the photoconductive gain (Γ), which is a physical quantity determining the efficiency of photocurrent generation or photocarrier collection of a photodetector, can be estimated according to the linear relationship with i_p

$$\Gamma = \frac{E}{e}\frac{i_p}{\eta P}, \quad (1)$$

where E is the photon energy, e is the unit electron charge, P is the incident optical power on the projected area (A) of the measured NRs and can be calculated as $P = IA = Iwl$, the w is the width of the NRs and l is the inter-distance between two contact electrodes of devices. To simplify the calculation, the quantum efficiency (η) is assumed to be unity. Physically, the Γ is proportional to the product of carrier lifetime (τ) and mobility (μ) and is written as $\Gamma = \tau\mu\,(V/l^2)$.[18-20]

The calculated Γ versus I of the NRs device with w = 300±60 nm and l = 2.0±0.2 μm is shown in the inset of Fig. 3(b). From the result, the Γ can reach a maximum at ~1000 under a low bias at 0.1 V and I = 100 Wm^{-2}. In addition, the Γ exhibits a near power-independent behavior, indicating the probable hole trapping mechanism. To further understand the PC mechanism, the environment-dependent PC measurement was also carried out. Figure 4 shows the photoresponse of the AlInN NRs enhanced by varying the environment from air to vacuum. The result reflects the surface-sensitive photoconductivity, which is somewhat similar to the oxygen sensitization (OS) PC mechanism in metal oxide semiconductor system such as ZnO, SnO^2, TiO_2, and WO_3.[21-25]

According to the OS model, the adsorbed oxygen molecules plays a role as the electron trap state on the surface and create upward surface band bending while capture electrons from the bulk. The photogenerated electrons and holes (either by bandgap or by sub-bandgap transition)[17] are separated by the surface band bending. The excess holes immigrate to the surface and recombine with the surface oxygen ion. The mechanism leaves the neutralized oxygen molecules and especially the unpaired electrons which predominantly contribute the photocurrent. As the electron lifetime is now decided by the oxygen desorption and readsorption rate, vacuum (oxygen-insufficient) ambience can

provide longer lifetime of electron than atmospheric air and thus enhances photocurrent of the NRs. A simple schematic for the PC mechanism is illustrated in Fig. 4(b). Furthermore, the capture (or recombination) of hole by surface oxygen ion is similar to the hole trapping mechanism in the bulk, which could also explain the near power-independent Γ (Fig. 3(b)) induced by the constant electron lifetime or hole trapping time.[21,24]

Recently, the vacuum-enhanced photoconductivity has also been observed for the binary III-nitride NWs such as InN[26] and AlNs.[17] The presence of native oxide on the nitride surface and the same upward surface band bending were proposed to explain the similarity of PC mechanism between the nitride and oxide nanomaterials. In addition, the negative photocurrent response in the wide-bandgap AlN NWs was not found for the AlInN NRs. The coexistence of electron trap and recombination center in the semiconductor is the criterion for negative PC to take place. The result implies the absence of the two defects or the different defect types in this wide-gap ternary nitride nanostructure.

In conclusion, the electronic transport properties of the ternary AlInN NRs grown by MSE technique have been investigated. The dark conductivity is estimated to be 15 $\Omega^{-1}cm^{-1}$. The shallow donor level/band with the activation energy at 11±2 meV is also obtained by the temperature-dependent measurement. In addition, the photoconductivity under UV illumination of the AlInN NRs has also been investigated. The gain of the NRs device is around 1000. The probable oxygen sensitization PC mechanism is proposed based on the observations of the power-independent gain and the ambience-dependent photocurrent.

Acknowledgements

The author RSC would like to thank the financial supports of the Taiwan National Science Council (Grant No. NSC 99-2112-M-011-001-MY3 and NSC 99-2738-M-011-001) and the National Taiwan University of Science and Technology (NTUST).

References

1. S. N. Mohammad, H. Morkoc, Prog. Quantum Electron. **20**, 361 (1996).
2. S. J. Pearton, J. C. Zolper, R. J. Shul, F. Ren, J. Appl. Phys. **86**, 1 (1999).
3. R. Butte, J. F. Carlin, E. Feltin, M. Gonschorek, S. Nicolay, G. Christmann, D. Simeonov, A. Castiglia, J. Dorsaz, H. J. Buehlmann, S. Christopoulos, G. B. H. von Hoegersthal, A. J. D.Grundy, M. Mosca, C. Pinquier, M. A. Py, F. Demangeot, J. Frandon, P. G. Lagoudakis, J. J. Baumberg, N. Grandjean, J. Phys. D: Appl. Phys. **40**, 6328 (2007).
4. Md. M. Satter, H. J. Kim, Z. Lochner, J. H. Ryou, S. C. Shen, R. D. Dupuis, P. D. Yoder, IEEE J. Quantum Electron. **48**, 703 (2012).
5. R. Butte, E. Feltin, J. Dorsaz, G. Christmann, J. F. Carlin, N. Grandjean, M. Ilegems, Jpn. J. Appl. Phys. **44**, 7207 (2005).
6. Z. T. Chen, S. X. Tan, Y. Sakai, T. Egawa, Appl. Phys. Lett. **94**, 213504 (2009).
7. S. Senda, H. Jiang, T. Egawa, Appl. Phys. Lett. **92**, 203507 (2008).
8. H. Sun, A. R. Alt, H. Benedickter, E. Feltin, J. F. Carlin, M. Gonschorek, N. Grandjean, C. R. Bolognesi, IEEE Electron Device Lett. **31**, 957 (2010).
9. S. Tirelli, D. Marti, H. Sun, A. R. Alt, J. F. Carlin, N. Grandjean, C. R. Bolognesi, IEEE Electron Device Lett. **32**, 1364 (2011).
10. J. Kuzmik, A. Kostopoulos, G. Konstantinidis, J. F. Carlin, A. Georgakilas, D. Pogany, IEEE Trans. Electron Devices **53**, 422(2006).
11. C. L. Hsiao, J. Palisaitis, M. Junaid, R. S. Chen, P. O. A. Persson, P. Sandstrom, P. O. Holtz, L. Hultman, J. Birch, Appl. Phys. Express **4**, 115002 (2011).
12. T. Seppanen, L. Hultman, J. Birch, Appl. Phys. Lett. **89**, 181928 (2006).
13. T. Seppanen, P. O. A. Persson, L. Hultman, J. Birch, G. Z. Radnoczi, J. Appl. Phys.

97, 083503 (2005).

14. B. T. Liou, S. H. Yen, Y. K. Kuo, Appl. Phys. A **81**, 651 (2005).
15. H. Y. Chen, R. S. Chen, F. C. Chang, L. C. Chen, K. H. Chen, Y. J. Yang, Appl. Phys. Lett. **95**, 143123 (2009).
16. C. Y. Chang, G. C. Chi, W. M. Wang, L. C. Chen, K. H. Chen, F. Ren, S. J. Pearton, Appl. Phys. Lett. **87**, 093112 (2005).
17. H. M. Huang, R. S. Chen, H. Y. Chen, T. W. Liu, C. C. Kuo, C. P. Chen, H. C. Hsu, L. C. Chen, K. H. Chen, Y. J. Yang, Appl. Phys. Lett. **96**, 062104 (2010).
18. R. S. Chen, H. Y. Chen, C. Y. Lu, K. H. Chen, C. P. Chen, L. C. Chen, Y. J. Yang, Appl. Phys. Lett. **91**, 223106 (2007).
19. P. Bhattacharya, Semiconductor Optoelectronic Devices (Prentice-Hall Inc., New Jersey, **1997**), Chap. 8, pp. 346-351.
20. M. Razeghi, A. Rogalski, J. Appl. Phys. **79**, 7433 (1996).
21. C. Soci, A. Zhang, B. Xiang, S. A. Dayeh, D. P. R. Aplin, J. Park, X. Y. Bao, Y. H. Lo, D. Wang, Nano Lett. **7**, 1003 (2007).
22. L. C. Hsu, Y. P. Kuo, Y. Y. Li, Appl. Phys. Lett. **94**, 133108 (2009).
23. C. H. Lin, R. S. Chen, T. T. Chen, H. Y. Chen, Y. F. Chen, K. H. Chen, L. C. Chen, Appl. Phys. Lett. **93**, 112115 (2008).
24. R. S. Chen, C. A. Chen, H. Y. Tsai, W. C. Wang, Y. S. Huang, J. Phys. Chem. C **116**, 4267 (2012).
25. K. Huang, Q. Zhang, F. Yang, D. He, Nano Res. **3**, 281 (2010).
26. R. S. Chen, T. H. Yang, H. Y. Chen, L. C. Chen, K. H. Chen, Y. J. Yang, C. H. Su, C. R. Lin, Nanotechnology **22**, 425702 (2011).

Figure Captions

Figure 1. (a) The typical cross-sectional view and top view (the inset) FESEM images of the vertically aligned AlInN NRs and **(b)** the XRD pattern of the as-grown AlInN NRs on VN(111)/sapphire(001) substrate.

Figure 2. (a) The selected dark current versus applied bias curves measured in the temperature range of 140–300 K and **(b)** the calculated conductivity versus temperature and its corresponding Arrhenius plot (the inset) for the AlInN NRs with w = 300±60 nm and l = 2.0±0.2 μm.

Figure 3. (a) The photocurrent response curves under different UV excitation intensity and **(b)** the photocurrent values versus light intensity and its corresponding PC gain (the inset) for the AlInN NRs with w = 300±60 nm and l = 2.0±0.2 μm.

Figure 4. (a) The typical photocurrent responses under 500 Wm^{-2} light intensity measured in air and vacuum ambiences for the AlInN NRs. **(b)** A schematic plot for the oxygen sensitization PC mechanism in the AlInN.

Figure 1, R. S. Chen *et al*

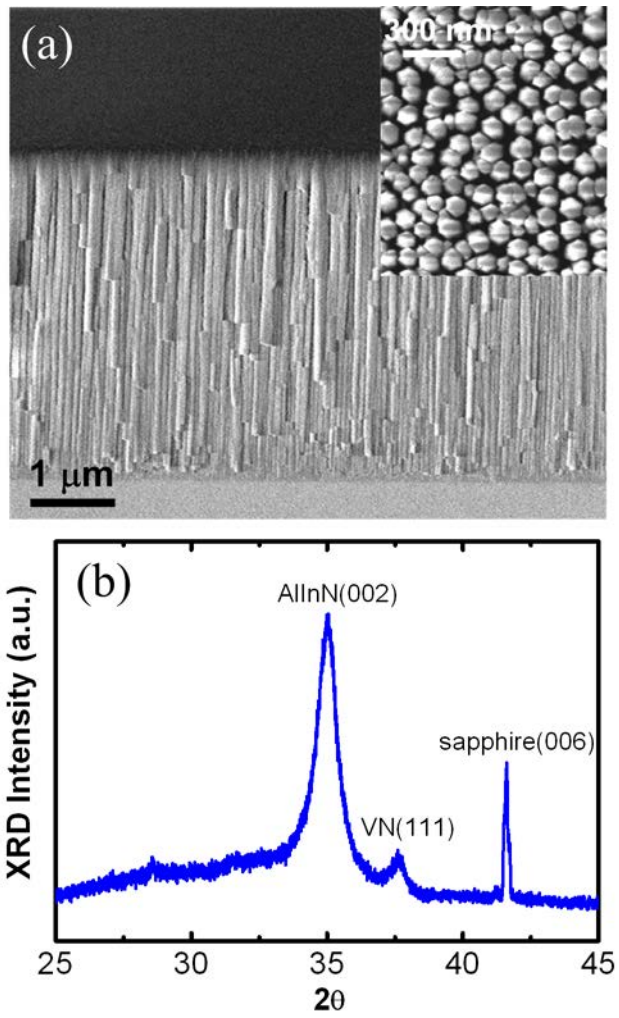

Figure 2, R. S. Chen *et al*

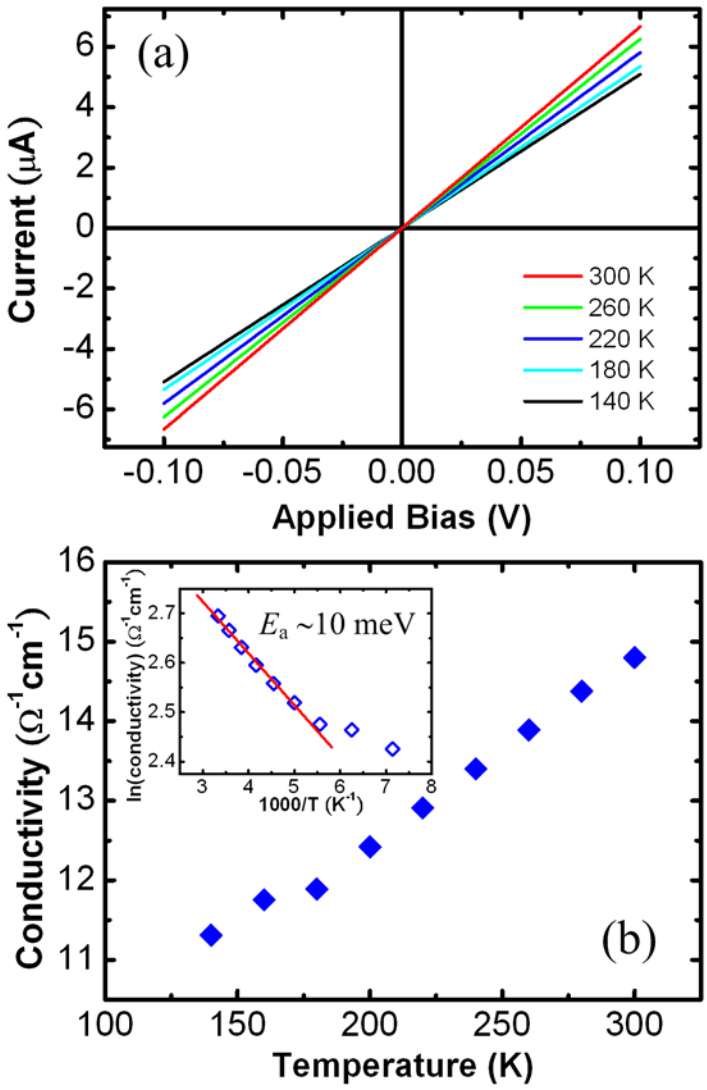

Figure 3, R. S. Chen *et al*

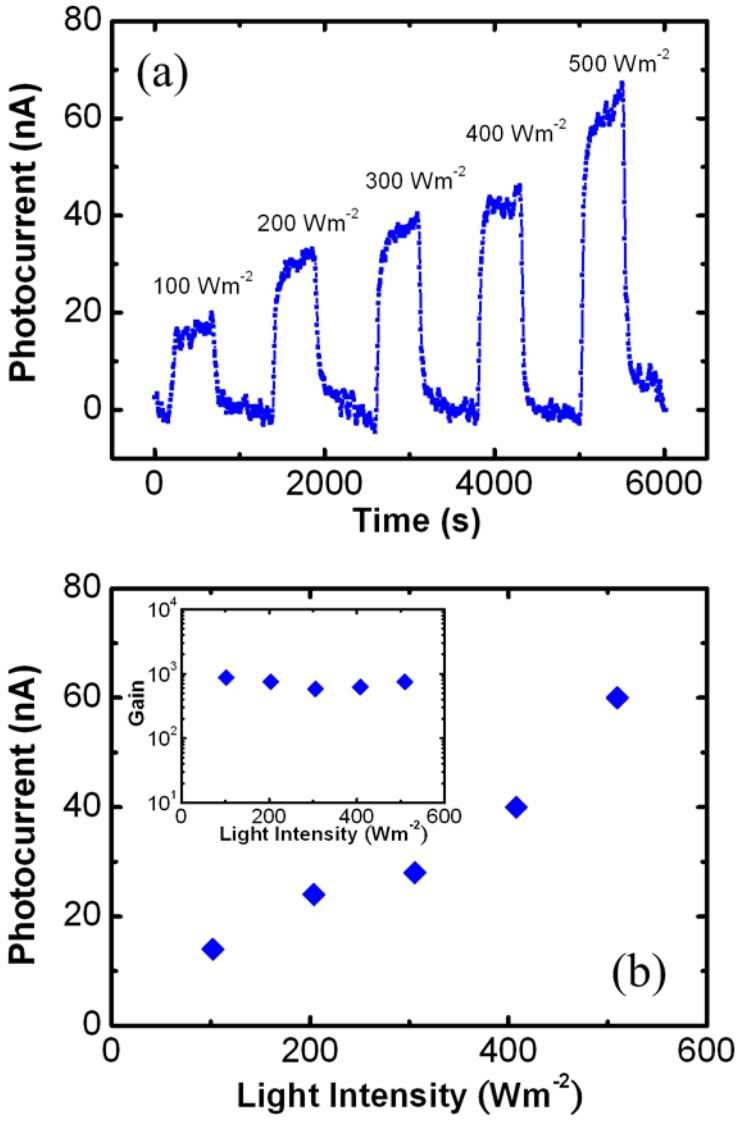

Figure 4, R. S. Chen *et al*